ACS Photonics

Article

pubs.acs.org/journal/apchd5

Self-Assembled Nanostructured Rear Reflector Designs for Thin-Film Solar Cells

Claire E. R. Disney,* Supriya Pillai, Craig M. Johnson, and Martin A. Green

Australian Centre for Advanced Photovoltaics, University of New South Wales, Sydney, NSW 2052, Australia

Supporting Information

ABSTRACT: To improve the competitiveness of solar cells, cell efficiency must increase and use of materials must be minimized. Light trapping measures can achieve this by allowing cells to absorb a greater fraction of the incident light. Traditional methods like surface texturing can negatively impact the cell's electrical characteristics and are generally unsuited to thin cell types. A plasmonic light trapping structure that avoids such issues can be formed using self-assembled hexagonal arrays of dielectric nanospheres in a continuous metal layer, at the rear surface of a cell. This can be easily fabricated toward the end of cell production, making it suitable for implementation with various solar cell types. 3D finite-difference time-domain simulations were conducted to investigate the potential of such structures, varying parameters including feature size and spacing, metal and absorber material and thickness, and the impact of random variations in the array. Significant improvements were found for a variety of topographies, with a peak increase in photocurrent from 2 μm silicon of 4.02 mA/cm^2 or 24.4%, relative to the case of a standard rear mirror with a 100 nm SiO_2 spacer layer. This also compares favorably to arrays of rear metal nanoparticles that previously yielded promising experimental results. We also identified critical parameters to control when designing such structures. A particular advantage of this structure is that it can offer light trapping advantages similar to those provided by metal nanoparticle arrays while still being able to serve as the rear contact of the cell due to the continuity of the metal layer.

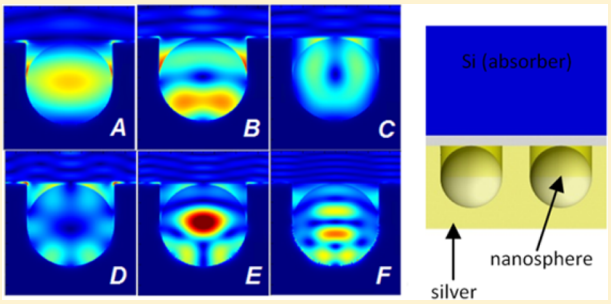

KEYWORDS: *simulation, plasmonics, light trapping, solar cells, FDTD, nanospheres*

With accumulating evidence supporting the anthropogenic nature of climate change, the shift toward more sustainable forms of energy generation is increasingly vital. Despite the accelerating deployment of renewable energy technologies, further improvements are still necessary in order to fully realize their potential. Solar energy converters can provide a cleaner alternative to traditional fossil fuels. However, despite strong growth in the solar industry in recent times, photovoltaic technologies still require significant cost reductions in order to be implemented on a grand enough scale to achieve the desired transformation in the energy industry.[1] In order to increase the efficacy of photovoltaic devices, the focus should be on developing methods of enhancing light absorption into the active layer while reducing the overall use of materials. Although bulk silicon (Si) cells have dominated the solar market, cells with a thinner active layer can have several key advantages and have attracted substantial interest.[2] However, optical absorption is low near the band-edge in both bulk and thin Si layers, due to the indirect band gap of the material. The penetration depth of light in this wavelength range can thus be significantly larger than the desired cell thickness.[3,4] This creates a trade-off whereby the increased absorption in thicker cells must be balanced against the need for thinner cells due to carrier diffusion lengths.[5]

Light trapping is one method for mitigating these optical losses and thus improving device performance. This allows for devices that are considered to be optically "thick" while maintaining thin physical dimensions. For bulk Si cells, this has traditionally been achieved through surface texturing, which increases the path-length of light through a cell and thus increases its chance of being absorbed.[6] However, texturing has various shortcomings that limit its utility, especially for thin-film cells, including increased surface recombination, relatively large feature size relative to cell thickness, deterioration of cell characteristics, and incompatibility with certain novel fabrication techniques.[7,8] Consequently, alternative methods of light trapping, including plasmonics, are of increased interest.

Plasmonic light trapping takes advantage of the fact that the nanoscale properties of metals differ from their bulk properties. Metallic nanostructures can preferentially scatter light into the solar cell's absorber due to resonant interaction with the incident light and thus increase light absorption.[9] This scattering is wavelength-dependent and the structures can be tuned to focus on wavelengths that are poorly absorbed.[10] A significant strength of these methods is that they should be able to exceed the theoretical limit of enhancement that texturing

Received: March 27, 2015
Published: July 7, 2015

DOI: 10.1021/acsphotonics.5b00153
ACS Photonics 2015, 2, 1108–1116

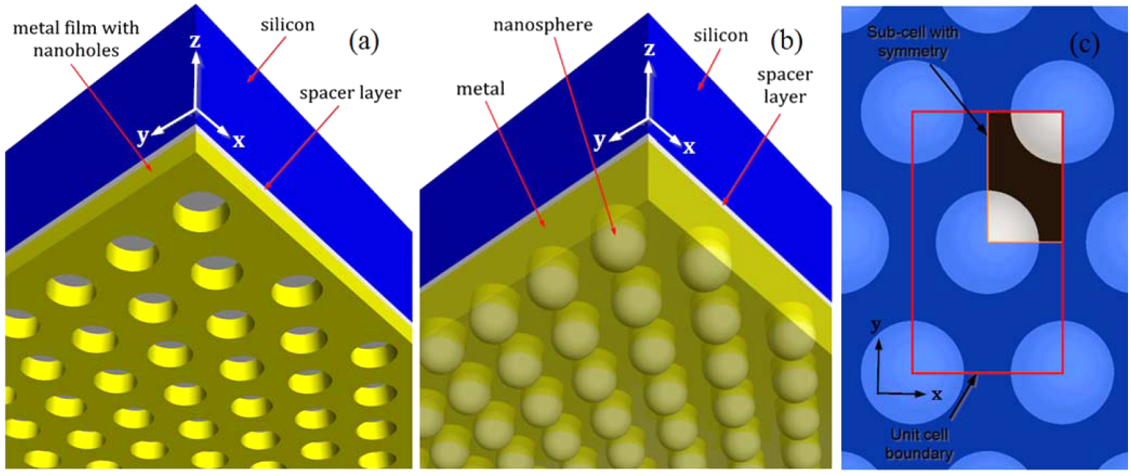

Figure 1. Isometric views of device structures investigated, thin crystalline silicon solar cells with a rear located SiO_2 spacer layer and metal film containing arrays of either (a) nanoholes or (b) dielectric nanospheres, and (c) plan view of the unit cell used in the simulations, including both the overall unit cell boundaries, and those of the subcell taking into account symmetrical boundary conditions.

could provide.[11] A wide variety of plasmonic structures have been considered for solar applications,[9] though many of these are still vulnerable to drawbacks or require complex or costly fabrication techniques. The use of self-assembled arrays of dielectric nanospheres to fabricate plasmonic rear reflectors has the potential to address some of these shortcomings.

The self-assembly of arrays of dielectric nanospheres is a well-established method for producing regular 2D arrays of nanoscale features.[12] Some key advantages of this method are its relative simplicity, large area application, and inexpensive nature, while still being able to tightly control the size and distribution of features.[13] Previous literature has demonstrated the use of such arrays in the fabrication of photonic crystals[14] and investigated the implementation of hexagonal tightly packed arrays of dielectric nanospheres (NSs) alone on the front and rear surfaces of solar cells for light trapping purposes.[4,15,16] These made use of the whispering gallery modes of the nanospheres to couple light into the adjacent absorber layer.

Here we consider rear placement of the NSs and the potential of varying their size and spacing by etching them after deposition. Following that, they can be coated with metal to create a metal/dielectric grating structure, or they can be etched away after metal deposition leaving a hexagonal array of nanoholes (NHs) in a metal film. These configurations are shown in Figure 1a–c. The interest in these two structures stems from previous work by Ferry et al., indicating enhanced light trapping in solar cells due to the generation of surface plasmon polaritons (SPPs) by arrays of nanofeatures on the interface between the rear surface of a solar cell and an adjacent metal film.[17] However, unlike the bottom up approach used in that work,[17] the technique proposed in this study could be used for any cell type without increasing the surface area of the semiconductor layer. These designs can be considered as a 2D photonic crystal with the associated potential for light trapping enhancement.[18] Depending on their morphology at the interface with the solar cell's active layer, such structures should be able to cause light of the desired wavelengths to be returned to the active layer at quite oblique angles leading to a significantly increased path length through the cell and greater chance for absorption.[19] When this angle exceeds the critical angle of the cell material, the light can subsequently be internally reflected, further increasing the chance of absorption. Nanohole arrays have also previously been found to potentially reduce transmission losses in thin metal films.[20,21] In such cases, shallow holes can lead to the generation of surface plasmons (SPs) at both surfaces coupled in such a way as to promote light scattering into the film, while for deeper holes the reverse is seen to be true as the SPs at the surface remain uncoupled from one another.[22]

The use of finite-difference time-domain (FDTD) simulations is a well-established technique for analyzing the optical behavior of solar cells.[23−25] In order to investigate the potential of self-assembled nanosphere-based rear reflectors, we undertook 3D simulations using Lumerical software.[26] The cases examined included densely packed hemispherical arrays of either embedded dielectric NSs, or NHs, both in a continuous metal layer at the rear of a thin crystalline silicon absorber, as shown in Figure 1a,b. For the NH arrays, the metal layer was set at 100 nm thick, whereas for the NS case the metal wholly coated the spheres and was modeled to be thick enough to be considered opaque. A silicon dioxide (SiO_2) spacer layer of 20 nm separated the Si and metal layers in accordance with our previous work.[27] The optical constants for each material were taken from literature.[28,29] Though we have recently contested Johnson and Christy's data,[30] this is a relative study and as such use of their data is suitable in the absence of a more accurate data set for silver. Periodic boundary conditions were utilized to allow the smaller unit cell shown in Figure 1c to simulate a wider array of the features. To measure absorption in Si and also parasitic absorption in metal, an unpolarized plane wave of wavelengths between 300 and 1200 nm illuminated the cell, with the results then integrated over the AM1.5 spectrum. The absorption into the silicon was isolated and from this the idealized photocurrent (J_{ph}) for each case simulated was calculated. This rests on the assumption that every photon absorbed generates an electron−hole pair that contributes to the external current, which allows us to compare the upper bound of performance in each simulated case neglecting recombination losses. Simulations were also conducted using semi-infinite nonabsorbing Si in order to identify scattering behavior from the rear interface and isolate the fraction of light incident on the rear surface that will be absorbed into the metal independent of the cell thickness.

DOI: 10.1021/acsphotonics.5b00153
ACS Photonics 2015, 2, 1108−1116

We base our design considerations on the experimental challenges that may be involved during fabrication. For the embedded NS arrays, models initially determined the impact of varying certain simulation parameters in order to more accurately replicate the real world implementation of these structures. This involved the inclusion or exclusion of a small air gap between the sphere and the solar cell due to line-of-sight issues in the application of the metal, as shown in Figure 2.

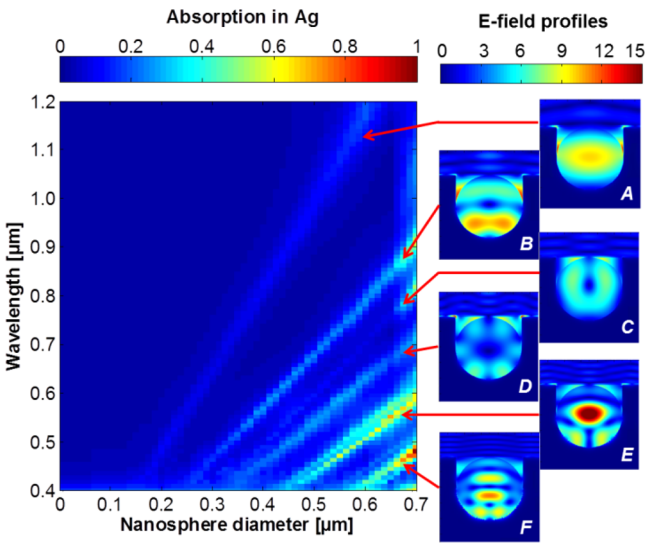

Figure 2. Absorption in Ag at the rear of nonabsorbing Si, for varying NS diameters with a 700 nm period. A diameter of zero corresponds to the case of a mirror. Absorption peaks reveal the emergence of multiple resonant modes that redshift with increasing NS size. Inset images show *Y*−*Z* cross sections of the electric field profiles associated with each of these modes (A−E).

Additionally, we considered the potential of "roughening" of the spheres that may occur due to the etching used to reduce the sphere diameter relative to the array period, as seen in our fabrication process. This also allows us to study the underlying mechanisms of the enhancement provided by these structures. Following this, we investigated the relationship between the size and the periodicity of the nanofeatures and the performance enhancement, the impact of the metal used, as well as the role of the thickness of the cell structure and the influence of interference effects. Furthermore, the consequences of introducing semirandom variations in feature size within an array were assessed.

When considering the potential impact of these structures a base case structure is needed to compare against. Most studies have chosen to compare their light trapping structures to the case of a slab of bare Si or other structure with no rear reflector. We feel that it is more accurate to compare our rear structures to the case of total rear metallization, as this gives a better approximation of the performance of an existing cell. As such, in this study a Si absorber with a rear Ag mirror separated by a 100 nm SiO_2 spacer layer is simulated, using the same simulation conditions, which can be reasonably assumed to be a standard reference cell structure.

CLARIFYING SIMULATION PARAMETERS

When optimizing the design of these structures, one must identify which aspects of the design are critical to ensure accurate simulation results. While modeling will always involve a certain degree of simplification, certain features must be included to achieve accuracy. Since certain features can dramatically increase the computational intensity of simulations, it is useful to determine the sensitivity of results to the inclusion of these features. This can also be useful in gaining an understanding of the mechanism of enhancement provided by these light trapping structures.

In addition to the simulations on a fixed thickness of Si, we also considered the structures on the rear of a semi-infinite slab of Si. This Si was modeled as nonabsorbing in order to more clearly identify the far field scattering profiles for each wavelength of light, and also the parasitic losses into the metal. Figure 2 shows the absorption into the metal for this case with varying NS diameters and a 700 nm period. Highly absorbing modes can be identified at various wavelengths, with these modes red-shifting as the NS diameter increases. These modes are identified and their associated electric field profiles are shown in the inset images A−E in Figure 2. The positioning and profiles of these modes are maintained in the case of finite thickness absorbing Si as used in the later models, although those occurring below a 600 nm wavelength are not relevant as below this wavelength little difference in the absorption into Si was observed compared to the mirror case. It is important to note that when the Si is absorbing, the total fraction of light absorbed is significantly reduced due to much being absorbed prior to reaching the rear surface, and additional interference bands create striations in the absorption. The absorption in the metal dominates for shorter wavelengths with high intensity modes concentrated at the metal/sphere interface As the wavelength increases, the lossy SPPs at the metal interface become less dominant, reducing parasitic absorption in the metal. Despite these modes being associated with higher absorption in the metal, they are also associated with regions of especially high absorption in the Si relative to the mirror case, particularly modes A and B. Thus, modes associated with high parasitic absorption can still have a positive rather than negative impact on the scattering profile of these reflectors as discussed later.

In our fabrication of these structures, we utilize evaporation to deposit the metal on top of the spheres, with the resultant metal layer limited by the line-of-sight nature of this technology. This causes a small air gap between the NS and the spacer layer, as shown in Figure 3a. As a result, the void in the metal has a half-capsule shape rather than being spherical. Similar air gaps have been previously observed in similar structures fabricated using SiO_2 nanospheres.[4] To determine the importance of this factor on the light trapping properties, we simulated the case of either ignoring this air gap or including it with the layout shown in Figure 3b. The exclusion of this air gap was found to result in significantly reduced J_{ph} as compared to the case where it is included. For example, for an array of 600 nm diameter NSs with a 700 nm period, the J_{ph} with air gaps was 2.62 mA/cm^2 or 15.12% higher than when they were excluded. The cause of this can be identified by studying these structures at the rear of nonabsorbing Si. Despite the lower absorption in the Ag for structures with no air gap shown in Figure 3b, there appears to be significantly reduced large angle scattering with no air gap, as shown in Figure 3c, as well as reduced SPP activity at the interface of the metal and Si shown in Figure 3d. While only the plots for the modes A and B, the most relevant to our wavelength range of interest, are shown here, similar trends persist across the entire spectral range of interest. These results are in agreement with previous work

DOI: 10.1021/acsphotonics.5b00153
ACS Photonics 2015, 2, 1108−1116

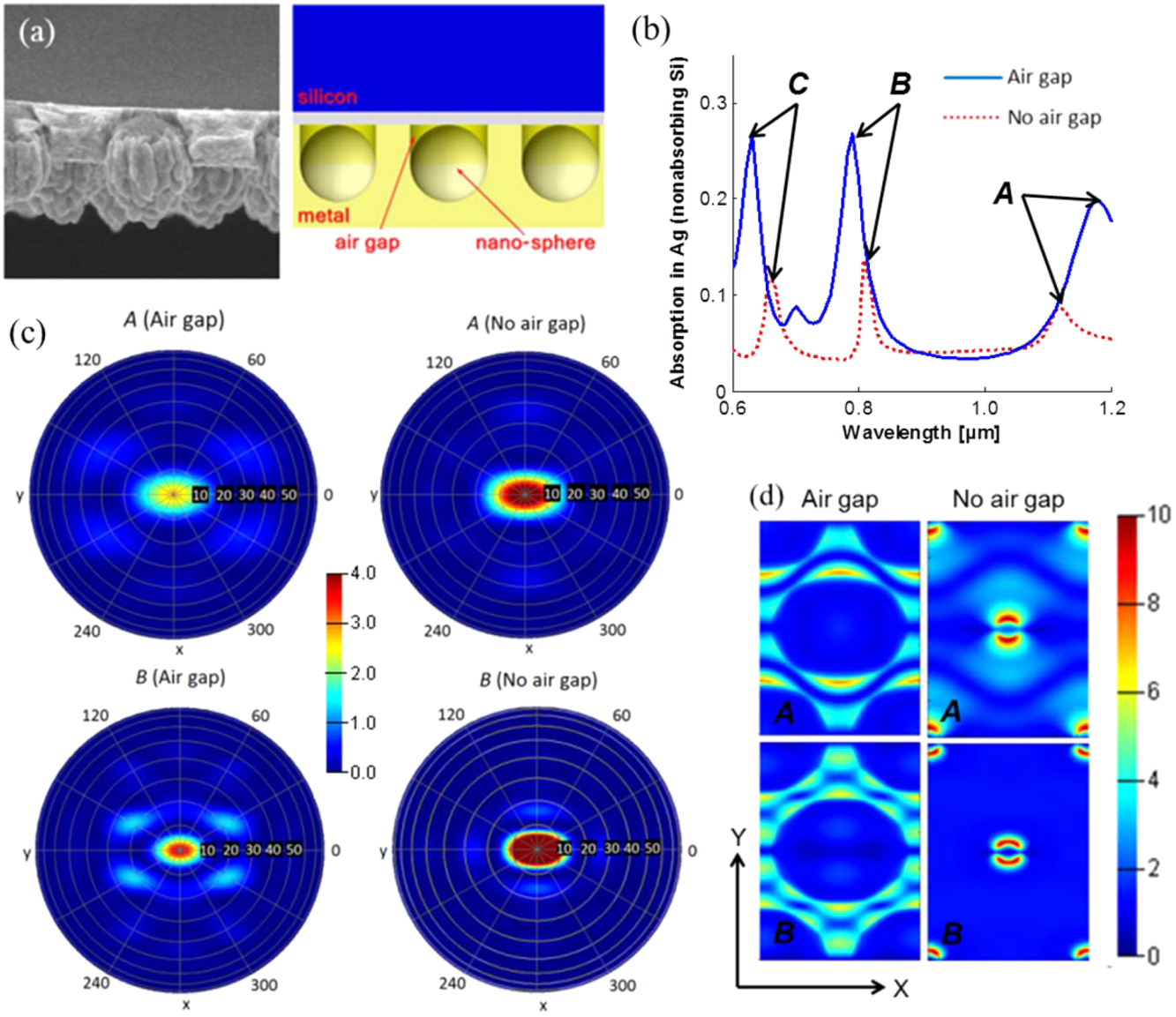

Figure 3. (a) SEM and simulated images of the rear surface of a Si cell with an array of polystyrene NSs coated in an Ag layer. Air gaps are evident between the Si and NS due to line of sight issues of applying the metal. (b) Absorption into Ag (c) far field scattering plots, and (d) $x-y$ cross sections of the electric field near the interface between the interface of the Si and Ag, all for 600 nm NSs on the rear of nonabsorbing Si with a 700 nm period, with or without the air gap shown in (a).

which found that spherical nanoscale voids in metal films produced reduced SPP related backscattering at the rim of the cavity as compared to hemispherical voids similar to our half-capsule shaped structures.[31] From this we conclude that the presence of this air gap is critical to accurately simulate the structures, as well as being vital to provide the desired morphology for scattering.

Subsequently, using the same structure geometry as in the previous case, we simulated the case where the SiO_2 spheres are not present, leaving only an empty void in their place. A small increase in J_{ph} from 2 μm Si of 0.33 mA/cm^2 was observed for the void-only case. This is only a ~1.6% increase, which appears to be related to the presence of the additional interface when the NSs are present. Such a structure could be fabricated, but the extra complexity seems unlikely to be warranted given the minimal increase in performance provided.

When fabricating these structures, polystyrene NSs as opposed to SiO_2 were initially tried. It was observed that the reactive ion etching (RIE) that is used to reduce the NSs to the desired diameter affected the morphology of the polystyrene spheres. Using this material, the resulting spheres after RIE will not have a smooth surface if etched for a long time, but rather have a roughened surface with multiple random protrusions and dimples, as shown in Figure S1. The longer the etch time, the greater the roughening effect, so for cases where the diameter is not much less than the period the spheres remain smooth, but when the diameter is a smaller fraction of the array period, the NSs take on a "popcorn" like porous texture.[32] It is expected that SiO_2 NSs would be more compatible with solar processing and may not have the same issues, and the effect does not occur at size combinations of the most interest to us. As such, the bulk of our simulations focus on smooth NSs. However, an analysis of the impact such roughening could have is shown in Figure S1.

DOI: 10.1021/acsphotonics.5b00153
ACS Photonics 2015, 2, 1108−1116

STRUCTURE OPTIMIZATION

After clarifying the layout and geometry of our simulations, it was possible to begin investigating the sensitivity of these structures' light trapping capability to variations in different parameters. As well as a comparison of the NH-based structures to the NS-based ones, we analyzed the role of the features size and array period, the impact of materials choices, and the effect of introducing a certain degree of randomness to the arrays. These allow for a deeper analysis of the potential of the structures and the dominant mechanism of enhancement provided by them.

Sensitivity to Size and Spacing Variations. As previously shown in Figure 2, the size of the spheres is particularly important in determining the location of modes A and B, associated with large-angle scattering. The link between array period and the modes was similarly investigated, and it was apparent that while the wavelength of each mode does remain fairly constant with increasing spacing, the strength of these modes decreases as the NSs are separated. Additionally, as the period increases, the scattering modes are not available, as the larger diffraction angles inhibit coupling into the Si, particularly at longer wavelengths.[34] These relationships are shown in Figure S2. As the NS size becomes close to the period, though the large angle scattering increases, absorption losses also increase with the emergence of extra leaky modes between adjacent spheres, tempering the possible photocurrent enhancement.

Initially, a wide variety of feature sizes and array periods were simulated both for the NS and the NH cases. A 2 μm thick Si absorber layer was used and Ag was selected for the metal choice as per the previous simulations, with contour plots of the resulting J_{ph} shown in Figures 4 and 5. In these plots, the result for a feature size of zero was taken to be equivalent to the rear Ag mirror case. As such, any configuration that results in a J_{ph} of less than 16.46 mA/cm^2 can be considered to have a negative impact relative to a planar mirror. Though there are certain similarities between the ideal feature size and period for both holes and NSs, there are significant differences in the magnitude of the enhancement as well as the absence of some peaks in the NH case that are present in the NS case. Additionally, the NSs only have a negative impact for a very small range of periods and, even then, only when the sphere size is almost equal to the array period, leaving the vast majority of configurations capable of providing enhancement relative to a mirror case. Conversely, a much wider variety of configurations results in a negative impact when NH arrays are considered. Uniformly across all periods considered, there was a negative enhancement when the NH diameter equaled the array period. This case is analogous to the use of rear metal nanoparticles (MNPs), as the holes are so large that only small "islands" of metal are left behind, barely connected by extremely thin bands of metal. The shape and size of the "islands" in this case are particularly different from an ideal MNP, and as such, they fail to provide the same degree of enhancement that those optimized MNPs would. There are also marked differences between the feature sizes and periods that provide the greatest enhancement. While the NH cases have lower absorption losses than the NS arrays, the holes are also affected by transmission losses and lack the same resonances shown by spherical voids. Both NS and NH structures had a peak enhancement for a period of 400 nm with 250 nm holes yielding a J_{ph} of 18.83 mA/cm^2 and 275 nm NSs yielding 20.14 mA/cm^2, representing an increase compared to the mirror case of 14.4 and 22.36%, respectively. These cases are both notable in that they are almost the inverse layout of both our recent work concerning anodized aluminum oxide[33] and a previously identified ideal geometry for a rear located square array of 200 nm diameter Ag nanoparticles with a 400 nm period.[34] The NSs exhibited an additional, and significantly broader, enhancement peak for intermediate periods in cases where the NS size was 100−200 nm less than the period. The peak enhancement in this region was for 600 nm NSs with a 700 nm period, a similar size to those found to show promise as a front surface light trapping structure, without metal coverage,

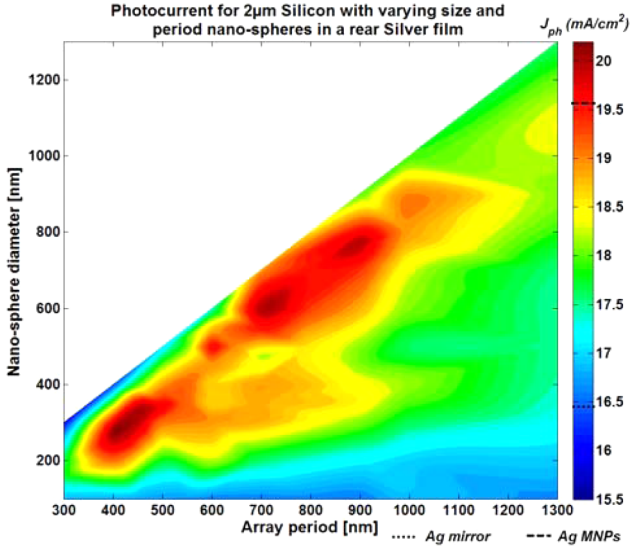

Figure 4. Photocurrent density (mA/cm^2) for a 2 μm Si absorber with NS diameters and periods in an Ag layer at the rear of the cell. The maximum J_{ph} is observed for a period of 400 nm with 275 nm NSs, and a similar peak for periods between ∼600−900 nm with NSs ∼ 100−200 nm smaller than the period. A variety of configurations show significant enhancement relative to the use of a rear mirror as a reflector.

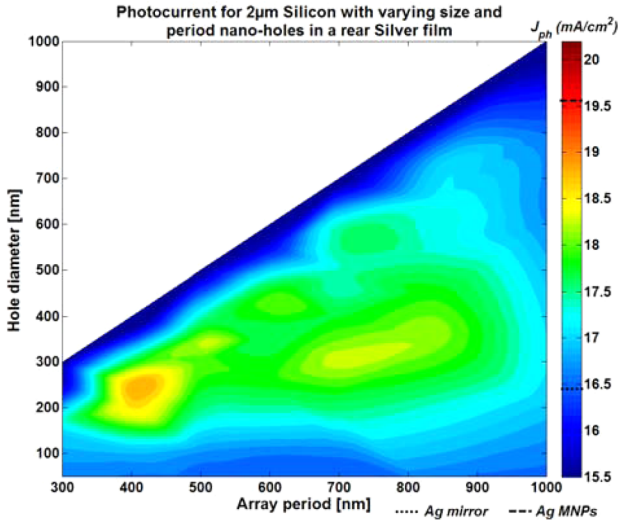

Figure 5. Photocurrent density (mA/cm^2) for a 2 μm Si absorber for varying NH diameters and periods in an Ag layer at the rear of the cell. The peak J_{ph} is observed for a period of 400 nm with 250 nm holes. Conversely to the NS structures, no second peak at larger periods is evident.

DOI: 10.1021/acsphotonics.5b00153
ACS Photonics 2015, 2, 1108−1116

in a previous study.[16] These larger period structures may be favorable for implementation due to the larger NSs they are formed from, increasing the practicality of their fabrication. Another reason the 700 nm period would be more suitable is that the absorption enhancement occurs strongly over a larger wavelength range, outperforming the 400 nm period structures in all but the shorter wavelength 600−700 nm light. The advantage of 600 nm NSs with a 700 nm period seems to be due to the ideal positioning of modes A and B, as shown in Figure 2, both of which are associated with large angle scattering, as well an SPP mode associated with strong large angle scattering lying between them. Absorption enhancement is particularly evident across the 800−1200 nm range, averaging 2.6× as much absorption as the mirror case. Although our base case was a rear mirror, we also simulated the same Si absorber with a rear square array of hemispherical Ag nanoparticles, using the 200 nm diameter and 400 nm period recommended by previous work.[34] This yielded a photocurrent of 19.57 mA/cm^2, which shows that for a variety of periods and diameters, the NS arrays will provide a favorable performance to these types of metal nanoparticles. In this way, these structures can provide the enhanced light trapping capability of metal nanoparticle arrays with the continuity of the metal given by mirrors, allowing it to provide both light trapping and the rear contact for the cell. As the NS size approaches 1 μm, higher order modes D−F redshift and enter our target wavelength range, these higher order modes are associated with greater absorption losses and narrower scattering, reducing light trapping and making NS sizes and periods of over 900 nm undesirable.

Notably, the NS arrays provide significant enhancement over the mirror for a much wider variety of configurations with relatively broad peaks in enhancement, reducing the sensitivity of their production. The NH arrays conversely seem more suited to either a front located light trapping structure or as an intermediate layer between two absorbers with the lower absorber making use of the substantial amount of light that can still be transmitted through this structure. The enhancement with either NSs or NHs can be attributed to different mechanisms of light trapping. Multiple different mechanisms come into play and the positive and negative effects of each balance out in differing ways with each configuration. The propagation of SPPs at the interface between the metal and Si may couple light into interface modes or waveguide modes, and the interplay between these can cause differing trends.[35]

Sensitivity to absorber material and thickness. As the assembly of these types of rear reflectors could be suited to thicker Si cells along with a variety of absorbers, it would be important to consider how these changes could impact the optimum size and spacing of the features. We simulated the NS array structures on 1 and 5 μm thick Si for a narrower band of periods in order to assess the impact of cell thickness on the enhancement potential of the devices. Figure 6a−c shows contour plots comparing the raw increase in J_{ph} over a mirror case for each thickness, which yielded 13.5 mA/cm^2 for 1 μm thick Si and 20.53 mA/cm^2 for 5 μm thick Si. As expected, the impact of varying the cell thickness differs depending on the spacing of the NSs, with the enhancements offered by the smaller NSs occurring at wavelengths too short to be of use for thicker cells.

A 500−600 nm spacing that is weaker for thinner cells due to lower enhancement in the 700−900 nm wavelength range than other periods, seemed more suited for use with thicker cells due to its higher absorption enhancement for wavelengths between 1000 and 1200 nm. Additionally, larger periods that place modes A and B at the borders of the desired wavelength range are likely to be the best choice, keeping the lossy modes out of this region. Though thickness of the cell affects destructive interference bands at certain wavelengths, these bands are narrow, whereas the absorption enhancement is over a broad range of wavelengths, meaning this should not be a factor in selecting the optimum size and period. For each thickness Si, J_{ph} achieved with the best performing NS arrays is equivalent to more than double the thickness of the Si with a rear mirror. Though thinner cells understandably experience a larger enhancement as a percentage of overall photocurrent, thick Si cells still absorb poorly in the near IR range, which could be enhanced with the addition of these rear reflectors, making it suitable for a variety of cell types, tailoring the positioning of the modes based on the material and thickness.

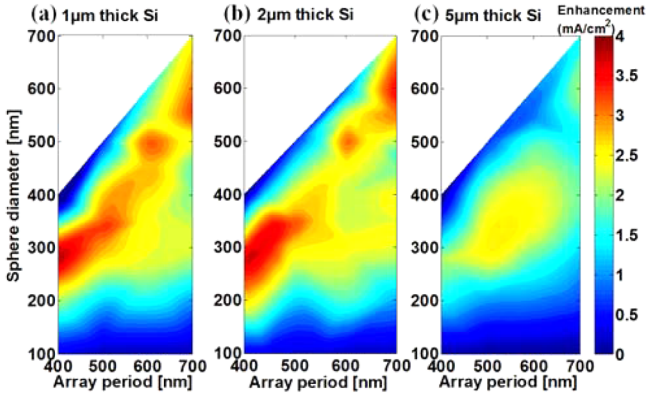

Figure 6. Calculated increase in J_{ph} compared to the use of a rear Ag mirror, for SiO_2 NS arrays of varying sizes and spacing, in an Ag layer at the rear of (a) 1 μm Si, (b) 2 μm Si, and (c) 5 μm Si. In addition to a shift in the optimum sphere diameter for a given period, the optimum period also varies depending on the cell thickness.

Sensitivity to Metal Choice. Although silver has been selected for the metal layer in all of the previous simulations, it is important to determine whether another metal might be more suitable. Despite its lower reflectivity than silver, previous work has made the case for using Al nanoparticles for light trapping,[36] as well as the well-established use of an Al layer at the rear of solar cells. Al provides significant cost and abundance advantages over Ag, and as such, both the NS and NH arrays were simulated to determine the impact on performance relative to Ag. However, as shown in Figure S3(a), the NS structures on Al perform significantly worse than the Ag ones. Offering at most a 6.44% enhancement to J_{ph} compared to an Ag mirror.

Despite this, there may be a number of cases in which Al would be an appropriate choice. First, if the NH arrays were being implemented on the cells front surface as previously suggested, the location of Al's resonance may make it less prone to suffering from destructive interference induced losses than Ag light trapping structures as previously noted with metal nanoparticles.[37] A key cause of the reduced performance seems to be excessive parasitic absorption into the metal at the 800−900 nm wavelength range as shown in Figure S3(b),(c), which would be less problematic for thicker cells making Al more appealing. Another prospective application for Al with such structures would be with non-Si absorbers.

DOI: 10.1021/acsphotonics.5b00153
ACS Photonics 2015, 2, 1108−1116

Sensitivity to Natural Variations within the Array and Non-normally Incident Light. Although this study thus far only modeled arrays with a single diameter of feature, in reality there will be some variation in the feature size and dislocations in the array. Previous research has indicated that randomly sized arrays of nanoparticles provided light trapping ability superior to those of uniform size.[38,39] In order to investigate the effect such topographies might have on our structures, we simulated arrays with a variety of feature sizes with layouts including those shown in Figure 7. A base case NSs with a 400

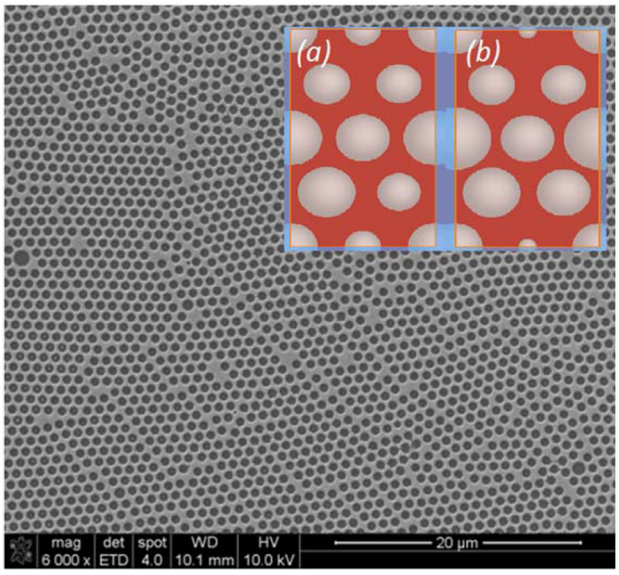

Figure 7. SEM image of an array of NHs in an Ag layer on a quartz substrate, showing some variations in feature size and dislocations in the array. (a, b) Unit cell layouts used to simulate the presence of multiple NS size within an array of between (a) 200−350 nm or (b) 100−400 nm.

nm period coated in Ag was considered. First, significant variations in feature size were modeled, with the minimum NS diameter being 200 nm and the maximum being 350 nm. There was little change in J_{ph} from 20.14 to 20.21 mA/cm^2. Subsequently, larger variations in size were modeled, with diameters between 100 and 400 nm in the one array. This further increased the J_{ph} to 20.48 mA/cm^2, which was the best result for any structure tested with this 2 μm thick Si, a 4.02 mA/cm^2 (24.4%) enhancement compared to the mirror case or 0.9 mA/cm^2 (4.7%) enhancement relative to the MNP array. There was strong enhancement across the full wavelength range of interest, particularly between 900 and 1200 nm. A comparison of the J_{ph} for the different rear reflectors is shown in Table 1. These results are in agreement with existing literature and suggest that the impact of random variations seen in real world implementation of this design should have an overall positive impact.

Another key advantage to these structures when performing under real world conditions is their wide acceptance angle for incoming light. While previous studies had noted omnidirectional enhanced absorption into metal films with the addition of nanovoids,[40] this occurred only over a narrow band of wavelengths and resonance for these sizes of voids lay in the short wavelengths already well absorbed by thin Silicon prior to reaching the rear surface. As a result, it was predicted that these structures should have enhanced scattering with low sensitivity

Table 1. Comparison of J_{ph} for Various Types of Rear Reflectors Simulated

rear reflector type	J_{ph} (mA/cm^2)	increase in J_{ph} relative to rear Ag mirror (%)
Al mirror (1 μm)	15.77	N/A
Ag mirror (1 μm)	16.46	N/A
275 nm NSs with 400 nm period in Al	17.52	6.44
250 nm NHs with 400 nm period in Ag	18.83	14.40
275 nm NSs with 400 nm period in Ag	20.14	22.36
semirandom array of NSs with 400 nm period in Ag	20.48	24.42
square array of 200 nm Ag NPs with 400 nm period	19.57	18.89

to the incoming angle of light. To test this, 2 μm Si with either a rear Ag mirror, or with embedded 275 nm NSs with a 400 nm period was simulated. The absorption into the Si as well as J_{ph} were analyzed for light incident from 0° (normal) to 70°. As shown in Figure 8a, there is a substantial enhancement to

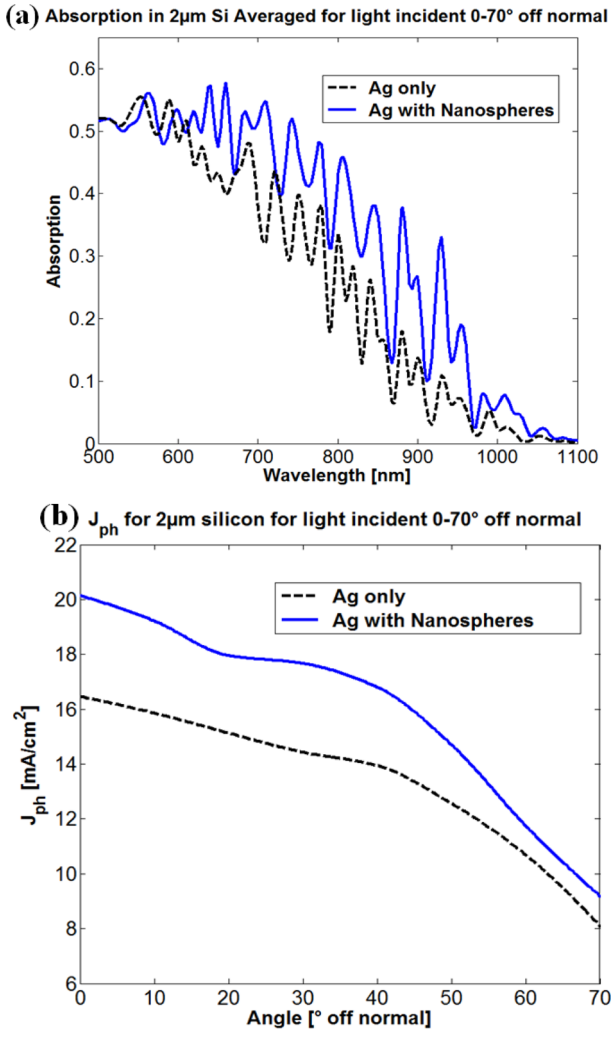

Figure 8. (a) Averaged absorption and (b) photocurrent for 2 μm silicon with either a rear silver mirror alone or including an array of 275 nm NSs with 400 nm period. Significant enhancement of absorption is evident leading to the higher J_{ph} across all angles.

DOI: 10.1021/acsphotonics.5b00153
ACS Photonics 2015, 2, 1108−1116

absorption in the Si with the addition of the NSs, causing a significant increase in J_{ph} relative to the mirror only case for all angles simulated shown in Figure 8b. The peak J_{ph} enhancement was 22.4% over the mirror case or an average enhancement across angles from 0 to 70° of ∼19%. The NH arrays similarly provided enhancement with varying angles of light. This further supports the suitability of these structures for utilization.

CONCLUSION

We assessed the light trapping potential of dielectric nanosphere and nanohole arrays in continuous metal films at the rear of solar cells. The results were encouraging, suggesting various configurations would provide significant photocurrent enhancement relative to rear mirrors or metal nanoparticle arrays. Despite several key plasmonic modes causing slightly elevated absorption in the metal, this is outweighed by the benefit of their accompanying large angle scattering and higher path length in the Si. Sensitivity to feature size and spacing proved to be moderate but important when considered in conjunction with the cell material and thickness. The rear film metal was an important design choice, with Ag offering significantly greater enhancement than Al. Several real-world factors impacted positively on structure performance, including the presence of an air-gap due to line of sight application of the metal and size variations within the array. The maximum increase in photocurrent observed for 2 μm thick Si using the embedded nanosphere structures was 4.02 mA/cm^2 (24.4%) relative to a rear mirror or 0.9 mA/cm^2 (4.7%) relative to the MNP array. These light trapping structures can be fabricated toward the end of cell production during metallization of the rear surface, without impacting on other processes, which makes them suitable for implementation on a variety of solar cell types. Another strong feature is their ability to combine significant J_{ph} enhancements relative to a rear mirror just as a nanoparticle arrays for light trapping would, while retaining the ability to be used as a rear contact for the cell, combining the respective advantages of both mirrors and MNP arrays. Overall, the NS arrays exhibit strong potential as a rear located light trapping structure for solar cells and warrants experimental investigation.

ASSOCIATED CONTENT

Supporting Information

(1) Surface roughening of polystyrene nanosphere arrays; (2) Nanosphere array period and its impact on plasmonic modes; (3) Aluminum rear reflectors with nanosphere arrays. The Supporting Information is available free of charge on the ACS Publications website at DOI: 10.1021/acsphotonics.5b00153.

AUTHOR INFORMATION

Corresponding Author

*E-mail: c.disney@unsw.edu.au.

Notes

The authors declare no competing financial interest.

ACKNOWLEDGMENTS

This Program has been supported by the Australian Government through the Australian Renewable Energy Agency (ARENA). The Australian Government, through ARENA, is supporting Australian research and development in solar photovoltaic and solar thermal technologies to help solar power become cost competitive with other energy sources. The views expressed herein are not necessarily the views of the Australian Government, and the Australian Government does not accept responsibility for any information or advice contained herein. We gratefully acknowledge the contribution of Qi Xu in production of SEM images.

REFERENCES

(1) Bagnall, D. M.; Boreland, M. Photovoltaic technologies. *Energy Policy* **2008**, *36*, 4390−4396.
(2) Rockstuhl, C.; Lederer, F. Photon management by metallic nanodiscs in thin film solar cells. *Appl. Phys. Lett.* **2009**, *94*, 213102.
(3) He, J.; Fan, C.; Wang, J.; Cheng, Y.; Ding, P.; Liang, E. Plasmonic Nanostructure for Enhanced Light Absorption in Ultrathin Silicon Solar Cells. *Adv. OptoElectron.* **2012**, *2012*, 592754.
(4) Eisenlohr, J.; Benick, J.; Peters, M.; Bläsi, B.; Goldschmidt, J. C.; Hermle, M. Hexagonal sphere gratings for enhanced light trapping in crystalline silicon solar cells. *Opt. Express* **2014**, *22*, A111−A119.
(5) Derkacs, D.; Lim, S.; Matheu, P.; Mar, W.; Yu, E. Improved performance of amorphous silicon solar cells via scattering from surface plasmon polaritons in nearby metallic nanoparticles. *Appl. Phys. Lett.* **2006**, *89*, 093103.
(6) Yu, Z.; Raman, A.; Fan, S. Nanophotonic Light-Trapping Theory for Solar Cells. *Appl. Phys. A: Mater. Sci. Process.* **2011**, *105*, 329−339.
(7) Catchpole, K. R.; Pillai, S. Absorption enhancement due to scattering by dipoles into silicon waveguides. *J. Appl. Phys.* **2006**, *100*, 044504.
(8) Ouyang, Z.; Pillai, S.; Beck, F.; Kunz, O.; Varlamov, S.; Catchpole, K.; Campbell, P.; Green, M. Effective light trapping in polycrystalline silicon thin-film solar cells by means of rear localized surface plasmons. *Appl. Phys. Lett.* **2010**, *96*, 261109.
(9) Atwater, H.; Polman, A. Plasmonics for improved photovoltaic devices. *Nat. Mater.* **2010**, *9*, 205−213.
(10) Beck, F.; Polman, A.; Catchpole, K. R. Tunable light trapping for solar cells using localized surface plasmons. *J. Appl. Phys.* **2009**, *105*, 114310.
(11) Yu, Z.; Raman, A.; Fan, S. Fundamental limit of nanophotonic light trapping in solar cells. *Proc. Natl. Acad. Sci. U. S. A.* **2010**, *107*, 17491−17496.
(12) Haynes, C. L.; Van Duyne, R. P. Nanosphere lithography: a versatile nanofabrication tool for studies of size-dependent nanoparticle optics. *J. Phys. Chem. B* **2001**, *105*, 5599−5611.
(13) Plettl, A.; Enderle, E.; Saitner, M.; Manske, A.; Pfahler, C.; Wiedemann, S.; Ziemann, P. Non-Close-Packed Crystals from Self-Assembled Polystyrene Spheres by Isotropic Plasma Etching: Adding Flexibility to Colloid Lithography. *Adv. Funct. Mater.* **2009**, *19*, 3279−3284.
(14) Ahn, S.; Kim, H.; Jeon, H.; Oh, J. R.; Do, Y. R.; Kim, H. J. Two-Dimensional Hexagonal Lattice Photonic Crystal Band-Edge Laser Patterned by Nanosphere Lithography. *Appl. Phys. Express* **2012**, *5*, 042102.
(15) Koh, W. S.; Akimov, Y. Enhanced light trapping in thin-film solar cells. *SPIE Newsroom* **2010**, 1−3.
(16) Grandidier, J.; Callahan, D. M.; Munday, J. N.; Atwater, H. A. Light Absorption Enhancement in Thin-Film Solar Cells Using Whispering Gallery Modes in Dielectric Nanospheres. *Adv. Mater.* **2011**, *23*, 1272−1276.
(17) Ferry, V. E.; Verschuuren, M. A.; Li, H. B. T.; Schropp, R. E. I.; Atwater, H. A.; Polman, A. Improved red-response in thin film a-Si:H solar cells with soft-imprinted plasmonic back reflectors. *Appl. Phys. Lett.* **2009**, *95*, 183503.
(18) Bermel, P.; Luo, C.; Zeng, L.; Kimerling, L. C.; Joannopoulos, J. D. Improving thin-film crystalline silicon solar cell efficiencies with photonic crystals. *Opt. Express* **2007**, *15*, 16986−17000.
(19) Sheng, P.; Bloch, A. N.; Stepleman, R. S. Wavelength-selective absorption enhancement in thin-film solar cells. *Appl. Phys. Lett.* **1983**, *43*, 579−581.

DOI: 10.1021/acsphotonics.5b00153
ACS Photonics 2015, 2, 1108−1116

(20) Braun, J.; Gompf, B.; Weiss, T.; Giessen, H.; Dressel, M.; Hübner, U. Optical transmission through subwavelength hole arrays in ultrathin metal films. *Phys. Rev. B: Condens. Matter Mater. Phys.* **2011**, *84*, 155419.
(21) Braun, J.; Gompf, B.; Kobiela, G.; Dressel, M. How holes can obscure the view: suppressed transmission through an ultrathin metal film by a subwavelength hole array. *Phys. Rev. Lett.* **2009**, *103*, 203901.
(22) Degiron, A.; Lezec, H. J.; Barnes, W. L.; Ebbesen, T. W. Effects of hole depth on enhanced light transmission through subwavelength hole arrays. *Appl. Phys. Lett.* **2002**, *81*, 4327−4329.
(23) Catchpole, K.; Polman, A. Design principles for particle plasmon enhanced solar cells. *Appl. Phys. Lett.* **2008**, *93*, 191113.
(24) Nagel, J. R.; Scarpulla, M. A. Enhanced absorption in optically thin solar cells by scattering from embedded dielectric nanoparticles. *Opt. Express* **2010**, *18*, A139−A146.
(25) Beck, F.; Mokkapati, S.; Polman, A.; Catchpole, K. Asymmetry in photocurrent enhancement by plasmonic nanoparticle arrays located on the front or on the rear of solar cells. *Appl. Phys. Lett.* **2010**, *96*, 033113.
(26) Lin, C.; Povinelli, M. The effect of plasmonic particles on solar absorption in vertically aligned silicon nanowire arrays. *Appl. Phys. Lett.* **2010**, *97*, 071110.
(27) Yang, Y.; Pillai, S.; Mehrvarz, H.; Kampwerth, H.; Ho-Baillie, A.; Green, M. Enhanced light trapping for high efficiency crystalline solar cells by the application of rear surface plasmons. *Sol. Energy Mater. Sol. Cells* **2012**, *101*, 217.
(28) Palik, E. D. *Handbook of Optical Constants of Solids*; Academic Press: New York, 1998.
(29) Johnson, P.; Christy, R. Optical Constants of the Noble Metals. *Phys. Rev. B* **1972**, *6*, 4370.
(30) Jiang, Y.; Pillai, S.; Green, M. A. Re-evaluation of literature values of silver optical constants. *Opt. Express* **2015**, *23*, 2133−2144.
(31) Cole, R. M.; Baumberg, J. J.; Garcia de Abajo, F. J.; Mahajan, S.; Abdelsalam, M.; Bartlett, P. N. Understanding Plasmons in Nanoscale Voids. *Nano Lett.* **2007**, *7*, 2094−2100.
(32) Akinoglu, E. M.; Morfa, A. J.; Giersig, M. Understanding anisotropic plasma etching of two-dimensional polystyrene opals for advanced materials fabrication. *Langmuir* **2014**, *30*, 12354−12361.
(33) Li, Y.; Dunham, S.; Pillai, S.; Ouyang, Z.; Barnett, A.; Lochtefeld, A.; Lennon, A. Design of Anodic Aluminum Oxide Rear Surface Plasmonic Heterostructures for Light Trapping in Thin Silicon Solar Cells. *IEEE J. Photovolt.* **2014**, *4*, 1212−1219.
(34) Mokkapati, S.; Beck, F. J.; Polman, A.; Catchpole, K. R. Designing periodic arrays of metal nanoparticles for light-trapping applications in solar cells. *Appl. Phys. Lett.* **2009**, *95*, 053115.
(35) Catchpole, K.; Mokkapati, S.; Beck, F.; Wang, E.; Mckinley, A.; Basch, A.; Lee, J. Plasmonics and Nanophotonics for Photovoltaics. *MRS Bull.* **2011**, *36*, 461−467.
(36) Akimov, Y.; Koh, W. Resonant and nonresonant plasmonic nanoparticle enhancement for thin-film silicon solar cells. *Nanotechnology* **2010**, *21*, 235201.
(37) Villesen, T.; Uhrenfeldt, C.; Johansen, B.; Hansen, J.; Ulriksen, H. Aluminum nanoparticles for plasmon-improved coupling of light into silicon. *Nanotechnology* **2012**, *23*, 085202.
(38) Wang, E. C.; Mokkapati, S.; Soderstrom, T.; Varlamov, S.; Catchpole, K. R. Effect of nanoparticle size distribution on the performance of plasmonic thin-film solar cells: Monodisperse versus multidisperse arrays. *IEEE J. Photovolt.* **2013**, *3*, 267−270.
(39) Pala, R. A.; Liu, J. S.; Barnard, E. S.; Askarov, D.; Garnett, E. C.; Fan, S.; Brongersma, M. L. Optimization of non-periodic plasmonic light-trapping layers for thin-film solar cells. *Nat. Commun.* **2013**, *4*, 2095.
(40) Teperik, T. V.; De Abajo, F. G.; Borisov, A.; Abdelsalam, M.; Bartlett, P.; Sugawara, Y.; Baumberg, J. Omnidirectional absorption in nanostructured metal surfaces. *Nat. Photonics* **2008**, *2*, 299−301.

DOI: 10.1021/acsphotonics.5b00153
ACS Photonics 2015, 2, 1108−1116